Applied Physics Letters ARTICLE scitation.org/journal/apl

Extrinsic n-type doping of Cd_3As_2 thin films

Cite as: Appl. Phys. Lett. **122**, 061901 (2023); doi: 10.1063/5.0133491
Submitted: 3 November 2022 · Accepted: 16 January 2023 ·
Published Online: 7 February 2023

View Online Export Citation CrossMark

A. D. Rice,[1,a)] J. N. Nelson,[1] C. Brooks,[2] S. Lany,[1,2] and K. Alberi[1]

AFFILIATIONS

[1]National Renewable Energy Laboratory, Golden, Colorado 80401, USA
[2]Department of Physics, University of Colorado, Boulder, Colorado 80309, USA

[a)]Author to whom correspondence should be addressed: Anthony.Rice@nrel.gov

ABSTRACT

Cd_3As_2 provides an excellent platform for studying the physics of three-dimensional Dirac semimetals due to its stability as well as its compatibility with thin film growth. Crystals made using both bulk and thin film synthesis are unintentionally doped n-type, and other than introducing Zn to reduce the carrier concentration, no efforts have been reported to alter this intrinsic doping without major changes to the band structure. Here, group VI elements Te and Se are introduced during epitaxy to increase the electron concentration of the films. Starting from an unintentionally doped electron concentration of $1–2 \times 10^{17}$ cm^{-3}, concentrations of up to 3×10^{18} cm^{-3} are achieved. Analysis of Shubnikov–de Haas oscillations reveals good agreement in calculated effective mass and Fermi velocity of highly doped films with unintentionally doped single crystals with similar electron concentrations. The density functional theory is also performed to study the effects of group VI substitutions and confirms no strong perturbations in the electronic structure. This work ultimately demonstrates tunability in the carrier concentration using extrinsic dopants without substantial changes in the band structure, allowing for intentional design of Fermi-level position for device applications.

Three-dimensional Dirac semimetals offer potential advantages for a number of technologies. Cd_3As_2[1–3] is a promising material in this regard, largely due to its compatibility with thin film synthesis and its similarity and compatibility with zinc blende semiconductors in both chemistry and structure.[4] Already, this material has been explored for several applications. It is currently being developed for photodetectors because of its broadband light absorption and fast carrier dynamics.[5,6] High phonon scattering and low thermal conductivity make it attractive for thermoelectrics.[7,8] Quantum confinement in thin layers opens a gap in the bulk states,[9] creating opportunities for manipulating electron spin within surface states.[10] Finally, gating has been explored to dynamically tune the carrier concentration in very thin films.[11] To fully realize the potential of bulk-like Cd_3As_2 epitaxial layers in devices, however, other ways to modify the intrinsic carrier concentration must be pursued.

Cd_3As_2 films[4] and bulk crystals[12] are intrinsically n-type. While the electron mobility is much higher than the hole mobility, electron concentrations are also much higher in these materials. Early studies attributed electron doping to As vacancies,[13] and more recent studies using scanning tunneling spectroscopy attributed conductance fluctuations to As vacancy clusters.[14] A recent density functional theory (DFT) and electronic structure study found that the intrinsic doping behavior is dominated by the balance between *n*-type Cd interstitials and *p*-type Cd vacancies.[15] While some works have been done to alter the electronic properties of Cd_3As_2, it has generally been confined to percent level alloying with isoelectronic cation and anion species. Adding Zn to the cation sublattice in low concentrations (<10%) reduces the electron concentration, while higher concentrations (>20%) induce a transition to a trivial semiconductor with p-type doping.[16] Analogous modifications have been performed in bulk single crystals.[17] Similarly, isovalent alloying of Sb on the anion sublattice has been shown to drive films p-type (>12%), it is achieved though here by increasing the band inversion.[18] Alloying of transition metals has also been explored in bulk crystals, including the use of Mn to slow down photocarrier dynamics,[19] Cr to create negative magnetoresistance,[20] and Eu to alter the magnetic properties.[21] However, in these cases, alloying changes the electronic structure beyond simply altering the carrier concentration. Extrinsic doping options, similar to those used in conventional semiconductors to achieve rigid band shifts, must be realized to fully design topological semimetals for device applications.

Here, n-type doping of Cd_3As_2 is achieved analogously using group VI elements to III–V compound semiconductors. Both Te and Se increase the electron concentration with minimal observable changes to the band structure. Starting at unintentionally doped

(UID) Hall concentrations as low as $1–2 \times 10^{17}$ cm^{-3}, electron concentrations as high as 3×10^{18} cm^{-3} are achieved. Attempts to dope above this value resulted in films with lower carrier concentrations and lower mobilities than expected. Lifshitz–Kosovich fitting is performed on Shubnikov–de Haas (SdH) oscillations to further understand the influence of the dopants on the Cd_3As_2 electronic structure. The effective mass and Fermi velocity values converge with calculated UID values in bulk single crystals. The mean free path also does not change with carrier concentration, suggesting that they are controlled by scattering events other than those associated with ionized dopants. Finally, we confirm the suitability of group VI elements as shallow donors via the density functional theory (DFT). Our results now demonstrate that it is possible to intentionally tune the electron concentration in arbitrary thick films.

Cd_3As_2 thin film structures were grown in a dual chamber, interconnected III–V, II–VI MBE system as described elsewhere.[22] All Cd_3As_2 films were grown in a (112) orientation on $Zn_{(1-x)}Cd_xTe$ buffer structures on GaAs(111) substrates using elemental sources and arsenic rich conditions. Te was added during Cd_3As_2 growth from a Knudsen cell, while un-cracked Se was provided via a valved cracker source. Magnetoresistance measurements were performed in a Physical Properties Measurement System from Quantum Design at temperatures from 300 down to 2 K and at fields of ±14 T on 6-point Hall bars fabricated using standard lithography techniques and Au contacts. Hall measurements were performed within a −0.1 to 0.1 T field range. SdH oscillations are extracted from the $\rho_{xx}(H)$ longitudinal resistivity data by simultaneously fitting $\rho_{xx}(H)$ at all temperatures to

$$\rho_{xx} = \rho_{osc} \times \rho_{BG} + \rho_{BG}, \tag{1}$$

where ρ_{BG} is a four term polynomial background and ρ_{osc} is the oscillatory part of the magnetoresistance following the standard Lifshitz–Kosevich form:[12,23]

$$\begin{aligned}\rho_{osc} &= \frac{\rho_{xx} - \rho_{BG}}{\rho_{BG}} \\ &= \left(\frac{\hbar\omega_c}{2A}\right)^{1/2} \frac{2\pi^2 k_B T/\hbar\omega_c}{\sinh 2\pi^2 k_B T/\hbar\omega_c} \\ &\quad \times e^{-2\pi^2 k_B T_D/\hbar\omega_c} \cos\left(\frac{2\pi F}{B} + \phi\right).\end{aligned} \tag{2}$$

A is a constant with dimensions of energy, F is the frequency of oscillations, k_B is the Boltzmann constant, T is the temperature, $\omega_c = eB/m^*$ is the cyclotron frequency, and m^* is the cyclotron effective mass. The Dingle temperature is $T_D = \hbar/(2\pi k_B \tau_Q)$, where τ_Q is the quantum lifetime. The resulting $\rho_{osc}(H)$ fits are used to extract the amplitude of SdH oscillations as a function of temperature, which are then fit to Eq. (2) at a fixed magnetic field with the maximum oscillation amplitude H_{max}. We iteratively fit until the values converge. We make the assumption of a linear Dirac-like dispersion typically used for Cd_3As_2 to determine the Fermi velocity $v_F = \hbar k_F/m^*$ and effective mass $m^* = E_F/v_F^2$, where E_F is the Fermi level.[12,23] Here, k_F is the Fermi crossing determined by the Onsager relation $F = \frac{\hbar}{2e}k_F^2$ between the SdH oscillation frequency and the cross-sectional area of the Fermi surface which we assume to be spherical and to have two identical copies. From this assumption, we extract the carrier concentration as

$$n_{3d,SDH} = \left(\frac{4}{3}\pi k_F^3\right)\frac{g_s g_v}{8\pi^3}, \tag{3}$$

where g_s is the spin and g_v is the valley degeneracy.

DFT calculations were performed for the 80 atom primitive cell of Cd_3As_2 using the strongly constrained and appropriately normed (SCAN) functional[24] and the projector augmented wave (PAW) method implemented in the VASP code.[25] A $4 \times 4 \times 4$ k-point mesh was used for Brillouin zone integration, and spin–orbit coupling was included. The Cd_3As_2 lattice was fully relaxed to its equilibrium bulk structure. The S, Se, and Te dopant substitutions were calculated for each of the three nonequivalent As sites. Atomic forces were converged to 0.01 eV/Å, and the cell-external lattice parameters were kept at their bulk values.

Figure 1 shows the temperature dependence of the carrier concentration [Fig. 1(a)], Hall mobility [Fig. 1(b)], and resistivity [Fig. 1(c)] for a number of Cd_3As_2 films doped with varying amounts of Se or Te. The starting UID n-type carrier concentration of $1–2 \times 10^{17}$ cm^{-3} is lower than most reports, especially compared to single crystals.[12] Mobility decreases at higher doping levels, typical of increased ionized impurity scattering by extrinsic dopants. The magnitudes of the temperature dependence of both properties decrease with higher doping levels, coinciding with an observed transition to metallic temperature dependence in resistivity beginning near 1×10^{18} cm^{-3}. Doping levels around 3×10^{18} cm^{-3} are ultimately achieved for both dopants. Attempts to dope films above this concentration with increased Se or Te flux were unsuccessful, resulting in films with lower carrier concentrations and even lower mobilities, typical of the formation of self-compensating point defects.

Figure 2 shows the relationship between the carrier concentration and Hall mobility at both 300 and 2 K. Data from UID Cd_3As_2 films are included as well. There is a pronounced relationship between the carrier concentration and mobility with the best mobility films also having the lowest carrier concentrations. Undoped films showed much larger differences between their 2 and 300 K mobility and concentration than the doped films [see Fig. 1(a)], suggesting a different scattering and electron donor mechanism than in the doped films. Data from bulk single crystals are also included. Bulk synthesis results in not only much higher electron concentrations but also much higher mobilities. Extended defects,[22] including dislocations,[26] primarily reduce mobilities in thin films, and despite strategies to reduce them, they are still the limiting factor in most reported values to date. While extended defect densities are lower in single crystals due to the lack of substrate, bulk synthesis is limited in its inability to control the chemical potential by finely tuning overpressures, likely resulting in a much larger population of electrically active point defects.

Additional information about the material properties is extracted from the high field magnetoresistance data shown in Fig. 3. ρ_{xx} curves of a highly Te-doped sample (2.4×10^{18} cm^{-3}) are shown in Fig. 3(a). They are similar to undoped samples with oscillations clearly visible at higher magnetic fields. The corresponding ρ_{xy} curves [Fig. 3(b)] are linear at all temperatures, and this linearity is observed for all samples. Kohler plots [Fig. 3(c)] are well behaved with higher doping leading to much lower thermal dependence on the carrier concentration, minimizing the difference between curves measured across the temperature range.[27] Highly doped films exhibit a polynomial trend in the magnetoresistance at lower fields with films transitioning or beginning to

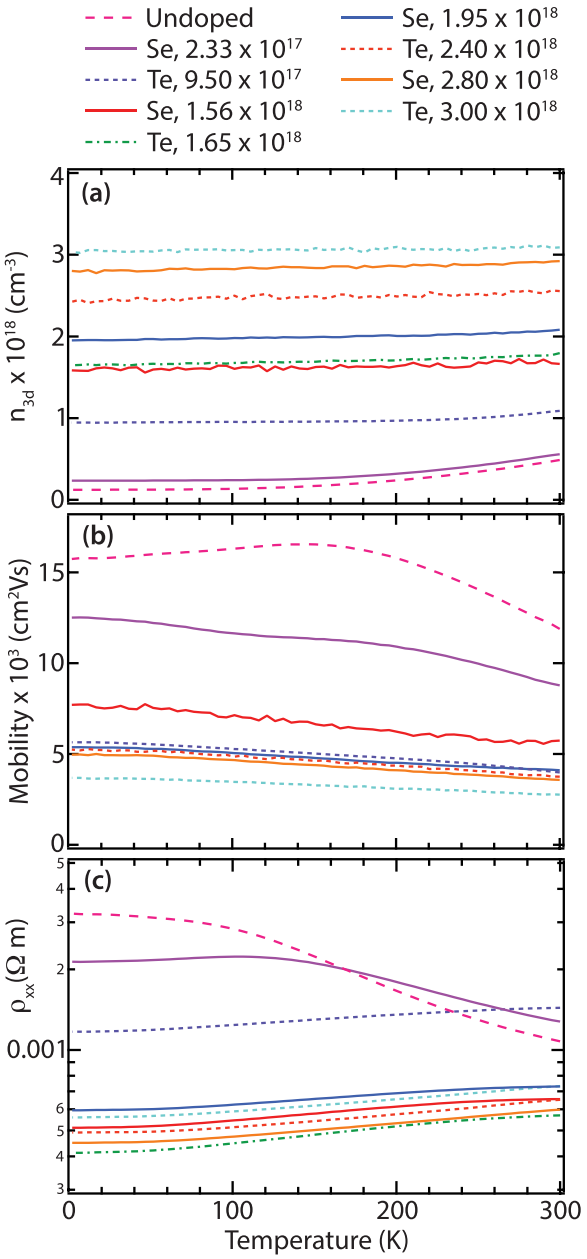

FIG. 1. (a) Hall carrier concentration, (b) Hall mobility, and (c) resistivity vs temperature of Cd_3As_2 films with varying degrees of Se and Te doping. Legend refers to dopant and measured carrier concentration at 300 K.

transition to a linear magnetoresistance trend at higher fields similar to UID Cd_3As_2 films.[28]

To further understand the effects of the dopants on the electronic structure of the films, SdH oscillations were extracted from the ρ_{xx} curves and fit using the Lifshiftz–Kosevich equation. As described earlier, we assume that the Fermi surface is spherical and a perfectly linear Dirac dispersion as is typical for Cd_3As_2.[12] Deviations from the simplified electronic structure, which are expected based on our DFT

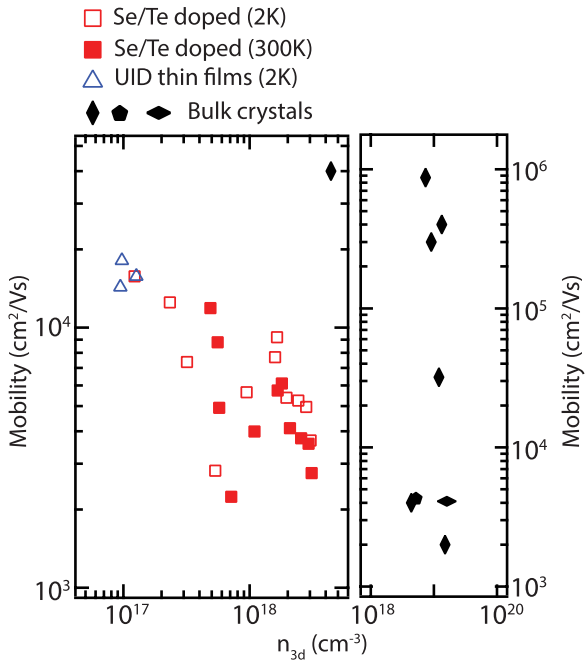

FIG. 2. μ vs n_{3d} for Se and Te doped films along with UID films grown under different As/Cd ratios and bulk single crystals (black pentagon,[3] vertical diamonds,[12] and horizontal diamonds[23]).

calculations, will cause the quantitative values to be slightly incorrect but do not impact the utility of this analysis in studying the sample to sample trends. An advantage of this approach is that it provides a way to compare these results with previously published bulk crystals. Figure 4(a) shows a typical extracted oscillation component as well as the fit. Figures 4(b)–4(d) summarize some of the extracted parameters

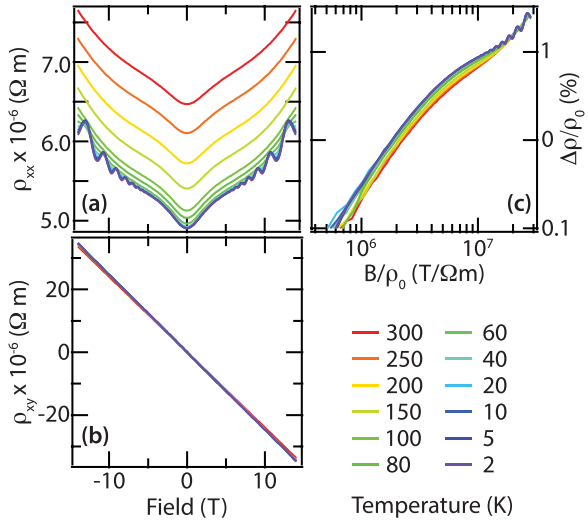

FIG. 3. Example (a) ρ_{xx}, (b) ρ_{xy}, and (c) Kohler plot for measurements taken between 2 and 300 K.

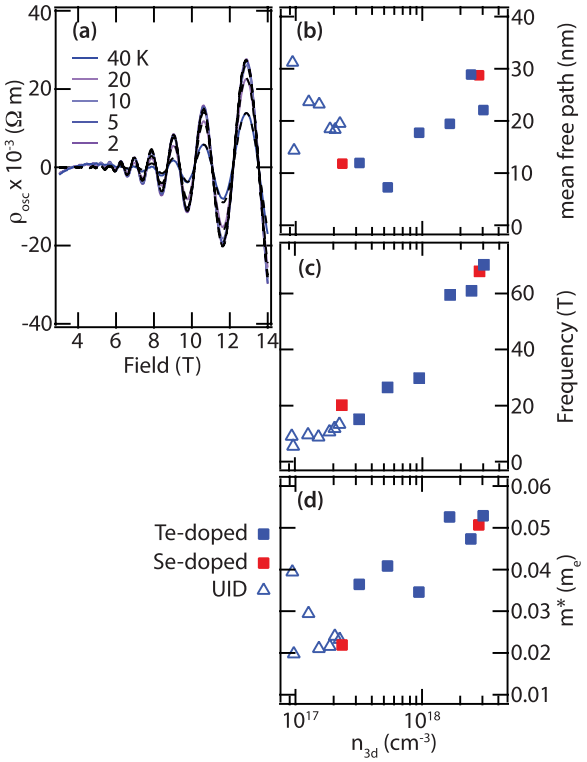

FIG. 4. (a) Typical SdH fitting for a standard Te doped film (2.4 × 10 18 cm^{-3}). Fits for each temperature are shown using dotted black lines. (b) Mean free path, (c) SdH frequency, and (d) effective mass, m∗, as a function of the measured Hall concentration for UID films and Se/Te doped films. Values are extracted from fitted SdH oscillations using the Lifshiftz-Kosevich formula.

as a function of the measured Hall carrier concentration. The mean free path [Fig. 4(b)], which is related to the quantum mobility rather than the Hall mobility, varies between 10 and 30 nm and shows virtually no trend across doping values, suggesting that this parameter is limited by scattering mechanisms completely separate from the effects of the added dopants. The extracted SdH oscillation frequency [Fig. 4(c)], which scales with the Fermi level, shows an expected monotonic, largely linear relationship with doping. The trend in the effective mass [Fig. 4(d)] is also consistent with values reported in the literature for Cd_3As_2 with varying electron concentrations. As expected, the Fermi velocity (not shown) is largely independent of the electron concentration and is consistent with bulk values at higher doping concentrations (9.9×10^5 m/s).[17] The similarities in these fundamental band structure properties between the intentionally doped films presented here and UID single crystals with similar electron concentrations suggest group VI elements shift the Fermi level position without substantially changing the fundamental band structure of Cd_3As_2.

The absence of strong perturbations of the electronic structure due to group VI doping is corroborated by the DFT-SCAN calculations. Figure 5 compares the total and site-projected DOS for doped and undoped Cd_3As_2. Due to ordering of the occupied cation sites on the underlying anti-fluorite lattice, three distinct As Wyckoff sites exist. Only the lowest energy group VI substitution is plotted in Fig. 5

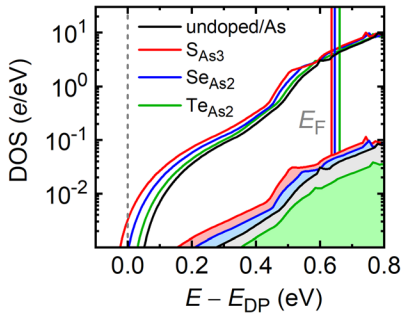

FIG. 5. Density of states calculated in DFT-SCAN in 80 atom cells of pure and doped Cd_3As_2. The As Wyckoff site with the lowest energy for substitution with group VI elements is indicated, and others are not plotted. The respective positions of the Fermi level are shown by the solid vertical lines. The shaded areas represent the site-projected local DOS for As, S, Se, and Te using an integration radius of 1 Å.

for simplicity as only minor differences between these sites are observed. The dopant substitution of one out of 32 As atoms per cell corresponds to a concentration of about three anion percent. Despite the high dopant concentration in the calculations, for all dopants, the total and local DOS closely resembles that of the undoped material, and the Fermi level increases more than 0.6 eV above the Dirac point energy, E_{DP} as expected for electron-donating dopants at this concentration. There are no indications of localized defect levels that would otherwise cause narrow peaked features in the DOS and pin E_F. However, there is a subtle but significant downward shift in the DOS above E_{DP}, also seen in the position of E_F. Consistent with expectations of chemical trends,[29] this effect is most pronounced for the sulfur dopant.

In conclusion, group VI elements, namely, Te and Se, are shown to be effective n-type dopants in Cd_3As_2, leading to increased electron concentrations. Films are doped to 3×10^{18} cm^{-3} before self-compensation via point defect generation is observed, and at these doping levels, no evidence is observed to suggest that the band structure is changing noticeably from intrinsic Cd_3As_2. The ability to intentionally tune the electron concentration is critical to device design efforts. This work also suggests that analogous attempts to lower the electron concentration via extrinsic doping with acceptors may be possible without percent level isovalent substitutions. Efforts to move the Fermi level closer to the Dirac point or even into the valence band will open up avenues for creating junctions and studying the physics of topological semimetals near the Dirac point.

This work was authored by the National Renewable Energy Laboratory, operated by Alliance for Sustainable Energy, LLC, for the U.S. Department of Energy (DOE) under Contract No. DE-AC36-08GO28308. Research was performed under the Disorder in Topological Semimetals project funded by the U.S. Department of Energy Office of Science, Basic Energy Sciences, Physical Behavior of Materials program. This research used high performance computing resources at the National Renewable Energy Laboratory, sponsored by the U.S. Department of Energy, Office of Energy Efficiency and Renewable Energy. The views expressed in the article do not necessarily represent the views of the DOE or the U.S.

AUTHOR DECLARATIONS

Conflict of Interest

The authors have no conflicts to disclose.

Author Contributions

Anthony Rice: Conceptualization (equal); Data curation (equal); Investigation (lead); Writing – original draft (lead). **Jocienne Nelson:** Formal analysis (lead); Investigation (equal); Writing – review & editing (equal). **Chase Brooks:** Methodology (equal). **Stephan Lany:** Methodology (lead); Writing – review & editing (supporting). **Kirstin M. Alberi:** Conceptualization (equal); Funding acquisition (lead); Investigation (supporting); Project administration (lead); Writing – review & editing (lead).

DATA AVAILABILITY

The data that support the findings of this study are available from the corresponding author upon reasonable request.

REFERENCES

[1]Z. Wang, H. Weng, Q. Wu, X. Dai, and Z. Fang, "Three-dimensional Dirac semimetal and quantum transport in Cd_3As_2," Phys. Rev. B **88**, 125427 (2013).
[2]M. N. Ali, Q. Gibson, S. Jeon, B. B. Zhou, A. Yazdani, and R. J. Cava, "The crystal and electronic structures of Cd_3As_2, the three-dimensional electronic analogue of graphene," Inorg. Chem. **53**, 4062 (2014).
[3]M. Neupane, S.-Y. Xu, R. Sankar, N. Alidoust, G. Bian, C. Liu, I. Belopokski, T.-R. Chang, H.-T. Jeng, H. Lin, A. Bansil, F. Chou, and M. Z. Hasan, "Observation of a three-dimensional topological Dirac semimetal phase in high-mobility Cd_3As_2," Nat. Commun. **5**, 3786 (2014).
[4]T. Schumann, M. Goyal, H. Kim, and S. Stemmer, "Molecular beam epitaxy of Cd_3As_2 on a III-V substrate," APL Mater. **4**, 126110 (2016).
[5]A. D. Rice, C. H. Lee, B. Fluegel, A. G. Norman, J. N. Nelson, C. S. Jiang, M. Steger, D. L. McGott, P. Walker, and K. Alberi, "Epitaxial Dirac semimetal vertical heterostructures for advanced device architectures," Adv. Funct. Mater. **32**, 2111470 (2022).
[6]Q. Wang, C.-Z. Li, S. Ge, J.-G. Li, W. Lu, J. Lai, X. Liu, J. Ma, D.-P. Yu, Z.-M. Liao, and D. Sun, "Ultrafast broadband photodetectors based on three-dimensional Dirac semimetal Cd_3As_2," Nano Lett. **17**, 834–841 (2017).
[7]H. Wang, X. Luo, W. Chen, N. Wang, B. Lei, F. Meng, C. Shang, L. Ma, T. Wu, X. Dai, Z. Wang, and X. Chen, "Magnetic-field enhanced high-thermoelectric performance in topological Dirac semimetal Cd_3As_2 crystal," Sci. Bull. **63**, 411–418 (2018).
[8]T. Zhou, C. Zhang, H. Zhang, F. Xiu, and Z. Yang, "Enhanced thermoelectric properties of the dirac semimetal Cd_3As_2," Inorg. Chem. Front. **3**, 1637–1643 (2016).
[9]T. Schumann, L. Galletti, D. A. Kealhofer, H. Kim, M. Goyal, and S. Stemmer, "Observation of the quantum Hall effect in confined films of the three-dimensional Dirac semimetal Cd_3As_2," Phys. Rev. Lett. **120**, 016801 (2018).
[10]W. Yanez, Y. Ou, R. Xiao, J. Koo, J. T. Held, S. Ghosh, J. Rable, T. Pillsbury, E. G. Delgado, K. Yang, J. Chamorro, A. J. Grutter, P. Quarterman, A. Richardella, A. Sengupta, T. McQueen, J. A. Borchers, K. A. Mkhoyan, B. Yan, and N. Samarth, "Spin and charge interconversion in Dirac-semimetal thin films," Phys. Rev. Appl. **16**, 054031 (2021).
[11]L. Galletti, T. Schumann, O. F. Shoron, M. Goyal, D. A. Kealhofer, H. Kim, and S. Stemmer, "Two-dimensional Dirac fermions in thin films of Cd_3As_2," Phys. Rev. B **97**, 115132 (2018).
[12]T. Liang, Q. Gibson, M. N. Ali, M. Liu, R. J. Cava, and N. P. Ong, "Ultrahigh mobility and giant magnetoresistance in the Dirac semimetal Cd_3As_2," Nat. Mater. **14**, 280 (2015).
[13]D. P. Spitzer, G. A. Castellion, and G. Haacke, "Anomalous thermal conductivity of Cd_3As_2 and the Cd_3As_2–Zn_3As_2 alloys," J. Appl. Phys. **37**, 3795–3801 (1966).
[14]S. Jeon, B. B. Zhou, A. Gyenis, B. E. Feldman, I. Kimchi, A. C. Potter, Q. D. Gibson, R. J. Cava, A. Vishwanath, and A. Yazdani, "Landau quantization and quasiparticle interference in the three-dimensional Dirac semimetal Cd_3As_2," Nat, Mater. **13**, 851 (2014).
[15]C. Brooks, M. van Schilfgaarde, D. Pashov, J. N. Nelson, K. Alberi, D. S. Dessau, and S. Lany, "Band Energy Dependence of Defect Formation in the Topological Semimetal Cd_3As_2" (unpublished).
[16]S. Nishihaya, M. Uchida, Y. Nakazawa, M. Kriener, Y. Kozuka, Y. Taguchi, and M. Kawasaki, "Gate-tuned quantum Hall states in Dirac semimetal $Cd_{1-x}ZnxAs_2$," Sci. Adv. **4**, eaar5668 (2018).
[17]H. Lu, X. Zhang, Y. Bian, and S. Jia, "Topological phase transition in single crystals of $Cd_{1-x}Zn_xAs_2$," Sci. Rep. **7**, 3148 (2017).
[18]Y. Nakazawa, M. Uchida, S. Nishihaya, M. Ohno, S. Sato, and M. Kawasaki, "Enhancement of spin-orbit coupling in Dirac semimetal Cd_3As_2 films by Sb doping," Phys. Rev. B **103**, 045109 (2021).
[19]Y. Sun, Y. Meng, R. Dai, Y. Yang, Y. Xu, S. Zhu, Y. Shi, F. Xiu, and F. Wang, "Slowing down photocarrier relaxation in Dirac semimetal Cd_3As_2 via Mn doping," Opt. Lett. **44**, 4103 (2019).
[20]H. Li, H. He, H.-Z. Lu, H. Zhang, H. Liu, R. Ma, Z. Fan, S.-Q. Shen, and J. Wang, "Negative magnetoresistance in Dirac semimetal Cd_3As_2," Nat. Commun. **7**, 10301 (2016).
[21]Y. V. Goryunov and A. N. Nateprov, "Influence of europium doping on magnetic properties of 3D topological semimetal Cd_3As_2 from ESR data," Phys. Solid State **60**, 68 (2018).
[22]A. D. Rice, K. Park, E. T. Hughes, K. Mukherjee, and K. Alberi, "Defects in Cd_3As_2 epilayers via molecular beam epitaxy and strategies for reducing them," Phys. Rev. Mater. **3**, 121201 (2019).
[23]L. P. He, X. C. Hong, J. K. Dong, J. Pan, Z. Zhang, J. Zhang, and S. Y. Li, "Quantum transport evidence for the three-dimensional Dirac semimetal phase in Cd_3As_2," Phys. Rev. Lett. **113**, 246402 (2014).
[24]J. Sun, A. Ruzsinszky, and J. P. Perdew, "Strongly constrained and appropriately normed semilocal density functional," Phys. Rev. Let. **115**, 036402 (2015).
[25]G. Kresse and D. Joubert, "From ultrasoft pseudopotentials to the projector augmented-wave method," Phys. Rev. B **59**, 1758 (1999).
[26]M. Goyal, S. Salmani-Rezaie, T. N. Pardue, B. Guo, D. A. Kealhofer, and S. Stemmer, "Carrier mobilities of (001) cadmium arsenide films," APL Mater. **8**, 051106 (2020).
[27]J. Xu, F. Han, T.-T. Wang, L. R. Thoutam, S. E. Pate, M. Li, X. Zhang, Y.-L. Wang, R. Fotovat, U. Welp, X. Zhou, W.-K. Kwok, D. Y. Chung, M. G. Kanatzidis, and Z.-L. Xiao, "Extended Kohler's rule of magnetoresistance," Phys. Rev. X **11**, 041029 (2021).
[28]A. Narayanan, M. D. Watson, S. F. Blake, N. Bruyant, L. Drigo, Y. L. Chen, D. Prabhakaran, B. Yan, C. Felser, T. Kong, P. C. Canfield, and A. I. Coldea, "Linear magnetoresistance caused by mobility fluctuations in n-doped Cd_3As_2," Phys. Rev. Lett. **114**, 117201 (2015).
[29]M. J. Caldas, A. Fazzio, and A. Zunger, "A universal trend in the binding energies of deep impurities in semiconductors," Appl. Phys. Lett. **45**, 671–673 (1984).